JOURNAL OF MATERIALS SCIENCE 21 (1986) 2475–2488

Toughening mechanisms in elastomer-modified epoxies

Part 2 *Microscopy studies*

R. A. PEARSON*, A. F. YEE‡
Polymer Physics and Engineering Branch, Corporate Research and Development, General Electric Company, Schenectady, New York 12301, USA

The toughening mechanisms of elastomer-modified epoxies are examined by scanning electron microscopy, transmission electron microscopy, and optical microscopy. DGEBA epoxies toughened by various levels of several types of carboxyl terminated copolymers of butadiene–acrylonitrile (CTBN) liquid rubber are studied. The materials are deformed in uniaxial tension and in three-point bending with an edge notch. Scanning electron microscopy of fracture surfaces indicate cavitation of the rubber particles to be a major deformation mechanism. Particle–particle interaction is also found. Optical microscopy of thin sections perpendicular to the fracture surface shows that the cavitated particles generate shear bands. The toughening effect is hypothesized to be due to cavitation, which relieves the triaxial tension at the crack tip, and shear band formation, which creates a large plastic zone.

1. Introduction

In a previous paper [1] two epoxide resin systems toughened with CTBN elastomers (carboxyl terminated copolymers of butadiene–acrylonitrile) were studied. Uniaxial tensile dilatometry was employed to elucidate the toughening mechanisms. The tensile dilatometry results indicate that the rubber particles enhance shear flow at low strain rates and promote cavitation when tested at high strain rates. Both mechanisms facilitate the shear localization process and result in enhanced toughness by the formation of a plastic zone ahead of the crack tip. This plastic zone efficiently blunts the sharp crack.

The purpose of this paper is to provide additional physical evidence that corroborates the deformation mechanisms deduced from our previous tensile dilatometry experiments. The nature of the plastic zones will be examined by a variety of microscopy techniques. Furthermore, the question of whether the stress whitened regions observed in the fractured specimens of elastomer-modified epoxides is due to massive crazing or simple void growth will be studied.

2. Experimental details

The preparation and mechanical testing of elastomer-modified epoxies has already been described in Part 1 of this series [1]. The specifications for the CTBN rubbers are listed in Table I. The composition of the various resins and the nomenclature used in this paper are listed in Table II. The fracture surfaces of tensile and single-edge notched three-point-bend (SEN-3PB) specimens of the neat and elastomer modified epoxies were examined using scanning electron microscopy (SEM). The instrument used was an ISI Super II scanning electron microscope. SEM specimens were coated with a thin film of Au–Pd alloy by sputtering. Also, backscattered electron imaging [2] was employed to locate the elastomer regions on the fracture surface of several rubber modified epoxies. These specimens were stained with an aqueous tetrahydrofuran (THF) solution of osmium tetroxide (OsO_4) and coated with a thin layer of carbon by evaporation. The electron-dense OsO_4 preferentially adds to the double bonds of the CTBN and provides contrast.

With few exceptions most solids do not fracture in the manner idealized by Griffith [3], because there is usually subsurface damage. The subsurface damage in these elastomer-modified epoxies were, therefore, examined by transmission optical microscopy (OM) and transmission electron microscopy (TEM). OM is useful for observing deformations that induce birefringence, voiding, and crazing. In order to view damage below the fracture surface, a thin section perpendicular to the fracture surface was obtained by metallographic thinning techniques [4]. Specimen preparation involves embedding the specimen in clear epoxy and then gradually producing a thin section by polishing the two sides perpendicular to the fracture surface, until a transparent slice in the centre remains. These sections, which are less than 25 μm in thickness, were viewed in a Zeiss microscope with transmitted light, with and without crossed polarizers.

TEM was performed on OsO_4 stained elastomer-modified epoxies in order to investigate the nature of

*Present address: General Electric Plastics Europe, PO Box 117 4600 AC Bergen op Zoom, The Netherlands.
‡Present address: Department of Materials Science and Engineering, University of Michigan, Ann Arbor, MI 48109, USA.

0022–2461/86 $03.00 + .12

TABLE I Specifications for the liquid rubber modifiers

	Hycar* CTBN		
	1300 × 15	1300 × 8	1300 × 13
Viscosity, Brookfield (mPa sec^{-1}) or cP at 27° C	55 000	125 000	625 000
Percentage carboxyl	2.47	2.37	2.40
Molecular weight	3500	3500	3500
Functionality	1.9	1.85	1.85
Acrylonitrile content (%)	10	17	27
Solubility parameter	8.45	8.77	9.14
Heat loss, 2 h at 130° C (%)	< 2.0	< 2.0	< 2.0
Specific gravity at 25° C/25° C	0.924	0.948	0.960

*Registered trademark.

the stress whitening seen in fractured specimens. The specimen preparation consists of potting the specimen in clear epoxy, some microtoming, staining with OsO_4 in an aqueous THF solution [5] and then obtaining thin sections (800 to 120 nm) cut perpendicular to the fracture surface. These thin sections were placed on copper grids and then examined using a Hitachi H-600 transmission electron microscope.

3. Results and discussion

In order to facilitate identification and discussion of the fractured tensile specimens and SEN-3PB specimens the schematic representation in Fig. 1 is used. The fracture surfaces of both types of specimens display distinct, visually observable regions. The fracture surface of SEN-3PB specimens contain 4 to 5 distinct regions: the saw cut, the razor cut, the starter crack, the stress-whitened zone when the epoxy is rubber modified, and the fast fracture zone which is almost mirror-like in appearance. The fracture surface of the tensile specimens are usually mirror-like in the case of the neat resins. In the case of elastomer-modified specimens distinct regions corresponding to slow and fast crack growth rates exist.

3.1. Scanning electron microscopy

The fracture surfaces of SEN-3PB specimens were examined using SEM. The neat epoxy 828 and 828-13(5), which is essentially a one-phase material, do not show any zones of stress-whitening. Except for a few large fracture steps, the fracture surfaces are basically featureless up to a magnification of 5000 ×, although some graininess approximately 0.1 μm in scale is discernible in 828-13(5) (Figs. 2 and 3). The absence of significant topographical features, in spite of the addition of CTBN rubber, correlates well with the lack of toughness.

When examining the fractured elastomer-modified SEN-3PB specimens by microscopy it is useful to describe the 3PB test. In the majority of cases the load rises linearly to a maximum, then drops as the crack propagates. During the rising load portion the elastomer-toughened specimens develop a stress-whitened zone ahead of the starter crack. For an unstable plane strain fracture the rising load portion accounts for the total energy to propagate a crack; thus, the stress-whitening is directly related to the energy absorbing mechanism.

The size of the stress-whitened zone increases with rubber content. G_{IC} also increases with increasing rubber content. The subsequent rapid crack propagation leaves a fracture surface without stress-whitening. Stress-whitening is due to the scattering of visible light from a layer of scattering centres, in this case voids. However, the absence of stress-whitening does not necessarily imply the absence of scattering centres,

TABLE II Composition and nomenclature of materials used (5phr* piperidine, Epon 828 resin used for all material)

Amount BPA (phr)*	Type of rubber	Amount of rubber (phr)*	Designation	T_g° C†
–	–	–	828	84.2
–	Hycar CTBN 1300 × 8	5	828-8(5)	–
–	Hycar CTBN 1300 × 8	10	828-8(10)	85.6
–	Hycar CTBN 1300 × 8	15	828-8(15)	–
–	Hycar CTBN 1300 × 8	20	828-8(20)	87.5
–	Hycar CTBN 1300 × 8	30	828-8(30)	82.4
–	Hycar CTBN 1300 × 15	5	828-15(5)	–
–	Hycar CTBN 1300 × 15	10	828-15(10)	84.2
–	Hycar CTBN 1300 × 15	15	828-15(15)	–
–	Hycar CTBN 1300 × 15	20	828-15(20)	89.4
–	Hycar CTBN 1300 × 15	30	828-15(30)	86.1
–	Hycar CTBN 1300 × 13	5	828-13(5)	–
24	–	–	828-BPA(24)	104.4
24	Hycar CTBN 1300 × 8	5	828-BPA(24)-8(5)	100.6
24	Hycar CTBN 1300 × 8	10	828-BPA(24)-8(10)	–
24	Hycar CTBN 1300 × 8	15	828-BPA(24)-8(15)	97.6
24	Hycar CTBN 1300 × 8	20	828-BPA(24)-8(20)	90.5

*phr; parts per hundred parts resin by weight.
†T_g was determined by DSC at 20° C min^{-1} from second heating.

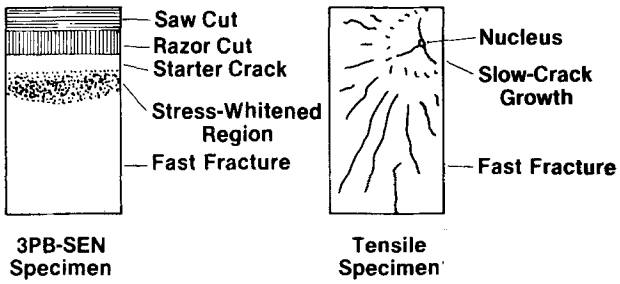

Figure 1 Schematic representation of fracture surface morphological features.

merely that the scattering layer is insufficiently thick, i.e. less than 1 μm.

The SEM details of the stress-whitened region of the elastomer-modified epoxies show that the rubber particles and the matrix have cavitated; and the diameters of the cavities in this region are greater than the diameters of the undeformed rubber particles as determined by TEM. In contrast, the cavities located in the fast fracture region are essentially the same size as the undeformed rubber particles. Evidence that these rubber particles have cavitated by cohesive failure will be presented later in this paper. The fracture surfaces of each rubber-modified epoxy system studied in this investigation are examined in the following sections.

The SEM micrographs of the stress-whitened regions on the fracture surfaces of the 828-15 materials are shown as a function of rubber content in Figs. 4 to 6. Aside from the increase in the density of void two features are noteworthy as the rubber content is increased. The first is that the voids become more uniform in size; the second is that the diameters become systematically larger. The first feature is simply due to the increase in uniformity of the rubber particles, while the second feature is probably due to

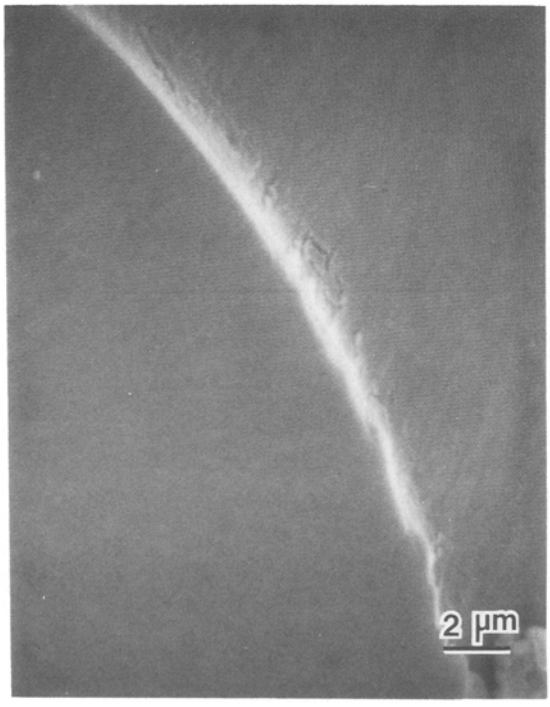

Figure 2 SEM of fracture surface of Epon 828 cured with piperidine.

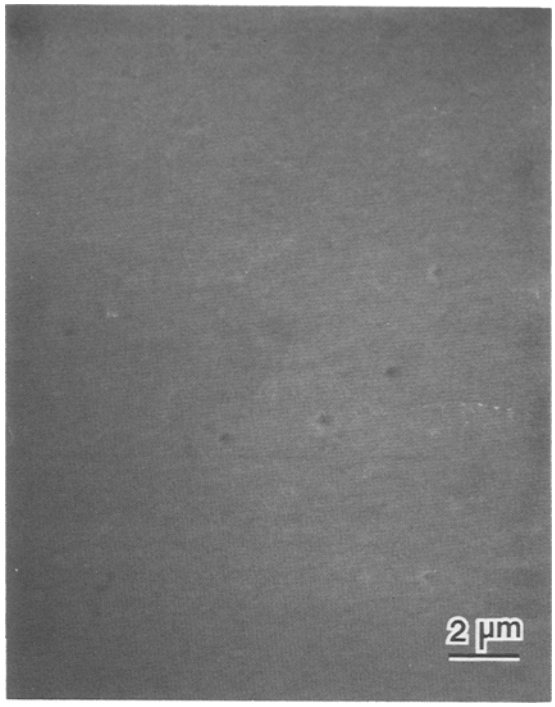

Figure 3 SEM of fracture surface of 828-13(5). No dispersed phase is present.

particle–particle interaction at high rubber concentrations. To provide further evidence for particle–particle interaction, a higher magnification SEM micrograph from the stress-whitened region of a SEN-3PB specimen of 828-15(30) is examined in Fig. 7. It is clear that the solid here resembles a closed-cell foam, and the voids are not spherical, but rather approach polyhedrons in shape. These polyhedral voids most likely began as spherical voids due to the net hydrostatic tension, but their growth became retarded as the voids began to "see" each other. Void growth due to a large

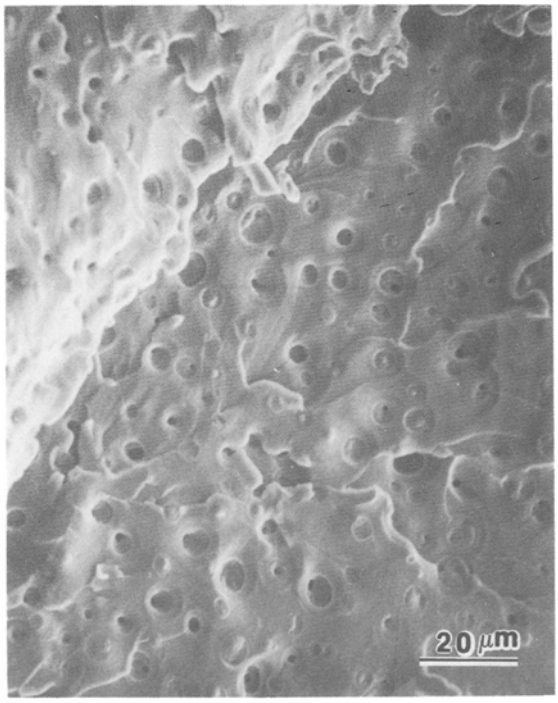

Figure 4 SEM from the stress-whitened area of fractured SEN-3PB specimen of 828-15(10). The white lines are due to tearing of the material between two crack planes, causing a surface step.

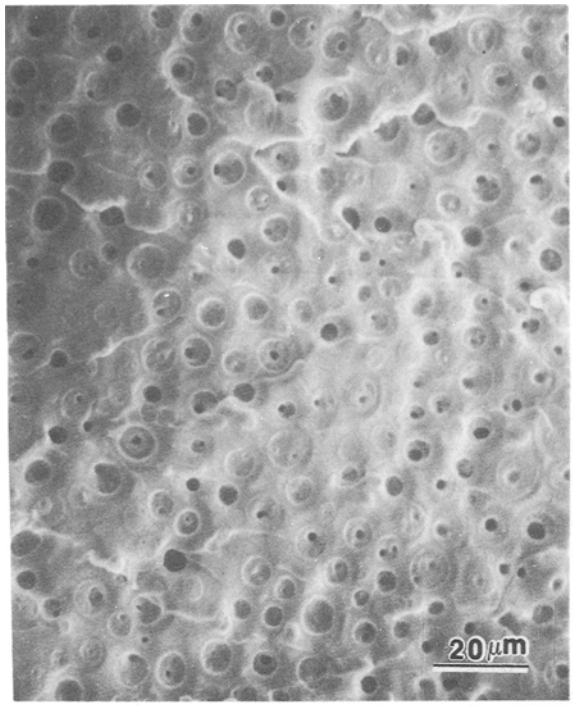

Figure 5 SEM from the stress-whitened area of fractured SEN-3PB specimen of 828-15(20).

shear stress would have resulted in elongated shapes. Most of the voids in Fig. 7 have a clearly defined hole at the centre. The matrix surrounding the voids exhibits notable plastic deformation as evidenced by the bevelled edges of the voids. The plastic deformation becomes larger as the particle–particle distance decreases: further evidence for particle–particle interaction. In Fig. 7, where the voids are quite close together, the bevelled edges actually intersect each other, forming fairly sharp ridges between neighbouring voids.

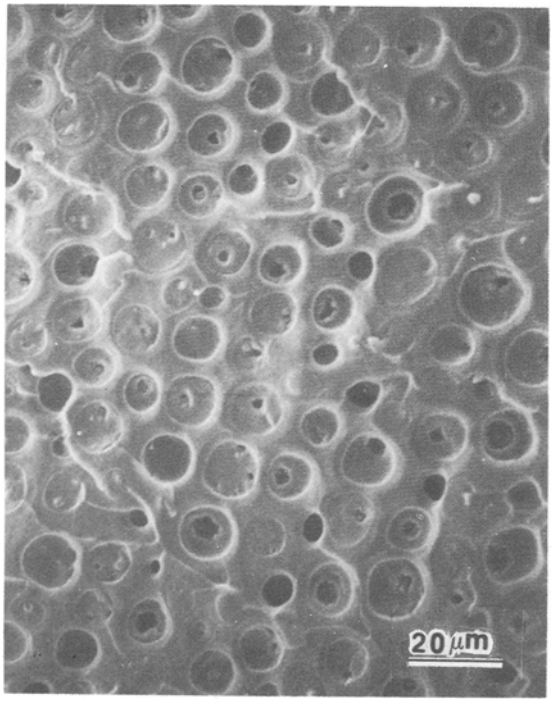

Figure 6 SEM from the stress-whitened area of fractured SEN-3PB specimen of 828-15(30).

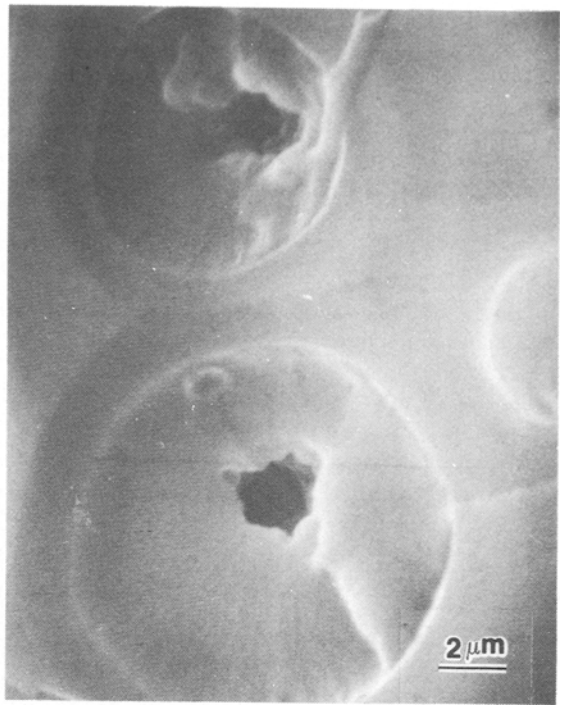

Figure 7 Higher magnification SEM of Fig. 6. Note the non-circular outline of the cavities due to particle–particle interactions. The edges of the cavities slope upward to meet the crack plane and form ridges.

The interaction between particles can also be seen by comparing the diameters of the fracture surface cavities (SEM) with the diameters of the undeformed rubber particles at various levels of rubber content (TEM). The analytical technique is described in Part 1 [1]. These results are shown in Fig. 8. It can be seen that in most cases the fracture cavities are larger than the corresponding rubber particles at the same rubber content. The expansion in the diameter in going from the undeformed state to the fracture cavity becomes more significant at increasing rubber content. The cavitation of the particles caused increases in diameter from ca. 50 to 200% in the case of the SEN-3PB fracture surfaces. The same figure shows that the diameter of the tensile fracture voids are larger than

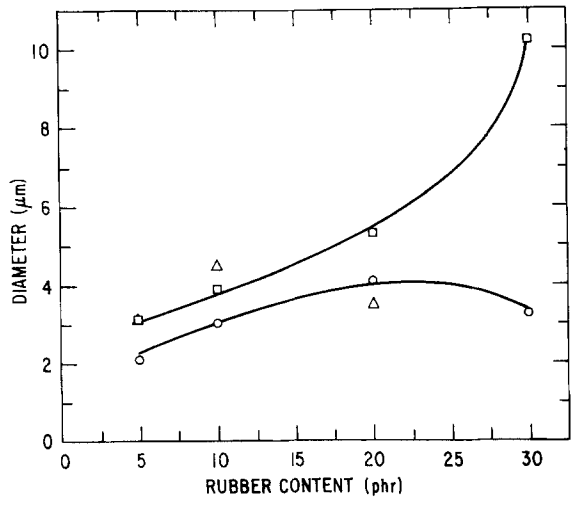

Figure 8 Dependence of diameters of rubber particles and fracture surface cavities on rubber content for the 828-15 system. (○) TEM, (□) SEM 3PB-SEN, stress-whitened area, (△) SEM, tensile specimen.

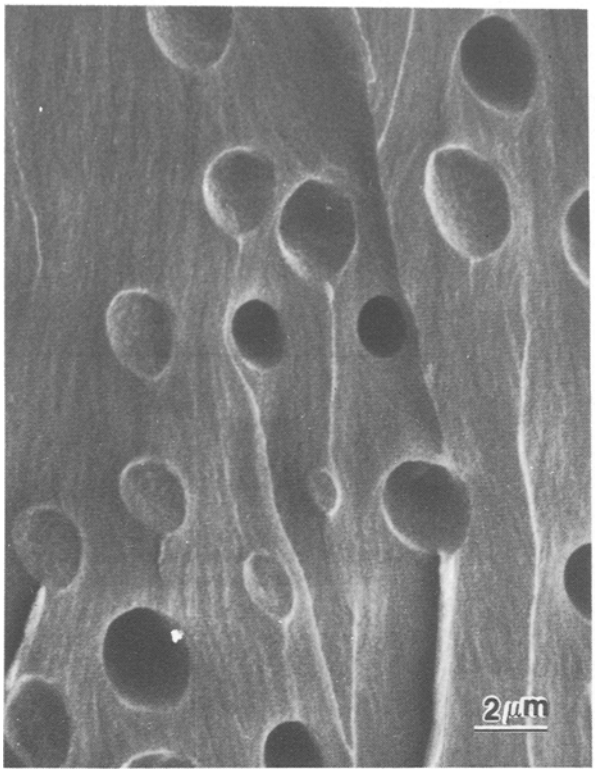

Figure 9 SEM from the stress-whitened area of fractured SEN-3PB specimen of 828-8(10). The striations have the same origin as those in Figure 4.

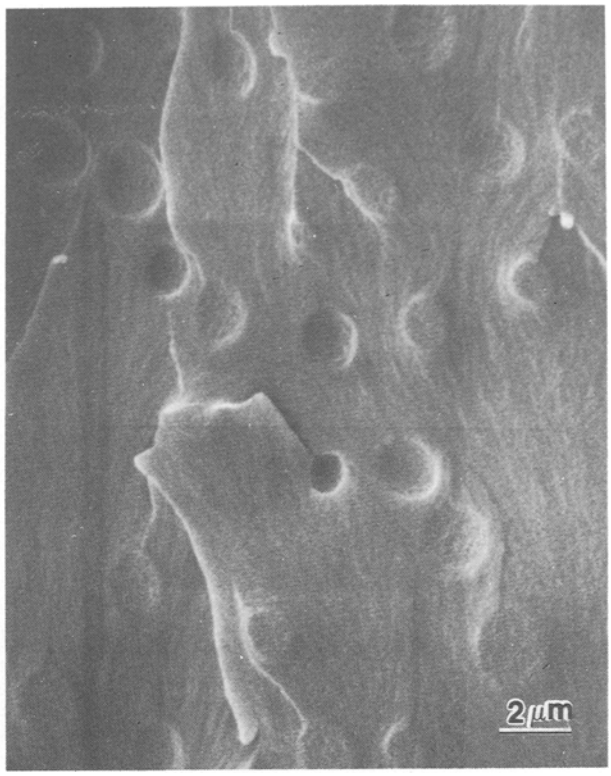

Figure 11 SEM from the fast fracture area of fractured SEN-3PB specimen of 828-8(10).

the undeformed particles by at least 50% at 5 and 10 phr rubber. However, at 20 phr the rubber particles are virtually unchanged in diameter to within measurement uncertainty. This is undoubtedly due to the fact that, according to the mechanical studies [1], at such a high rubber content the tensile deformation is essentially by shear.

Figs 9 to 12 are SEM micrographs from the stress-whitened (slow crack growth) and fast crack growth regions of the SEN-3PB fracture surfaces of the 828-8 system. The fast crack growth regions show very shallow disc-shaped cavities. The cavities found in the slow crack growth regions are larger than those in the fast crack growth regions. This was also observed for

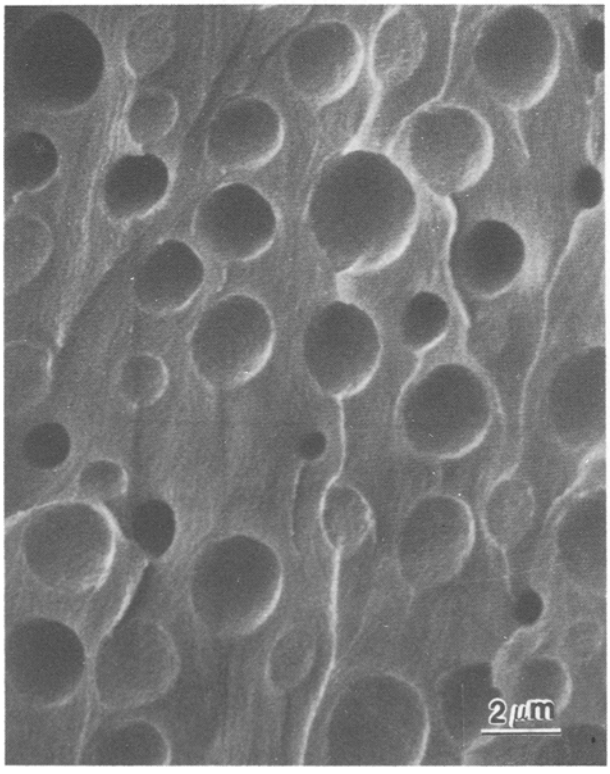

Figure 10 SEM from the stress-whitened area of fractured SEN-3PB specimen of 828-8(20).

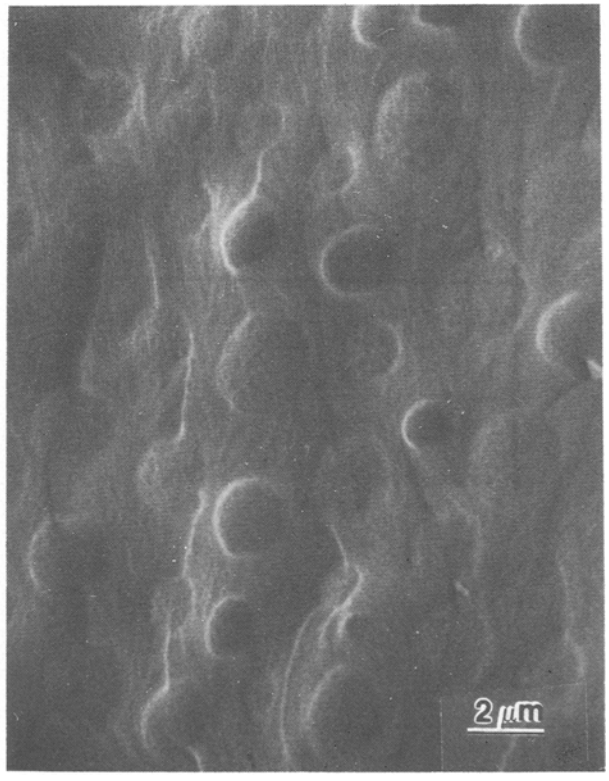

Figure 12 SEM from the fast fracture area of fractured SEN-3PB specimen of 828-8(20).

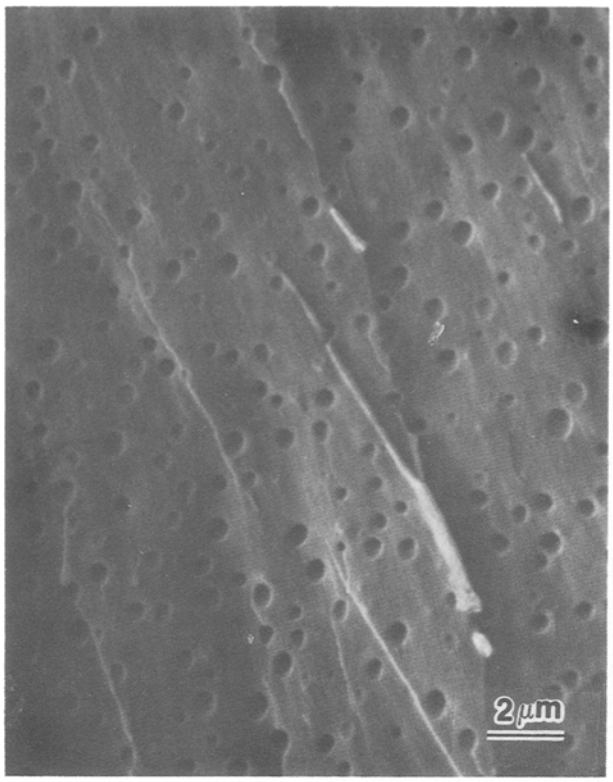

Figure 13 SEM from the stress-whitened area of fractured SEN-3PB specimen of 828-BPA(24)-8(5).

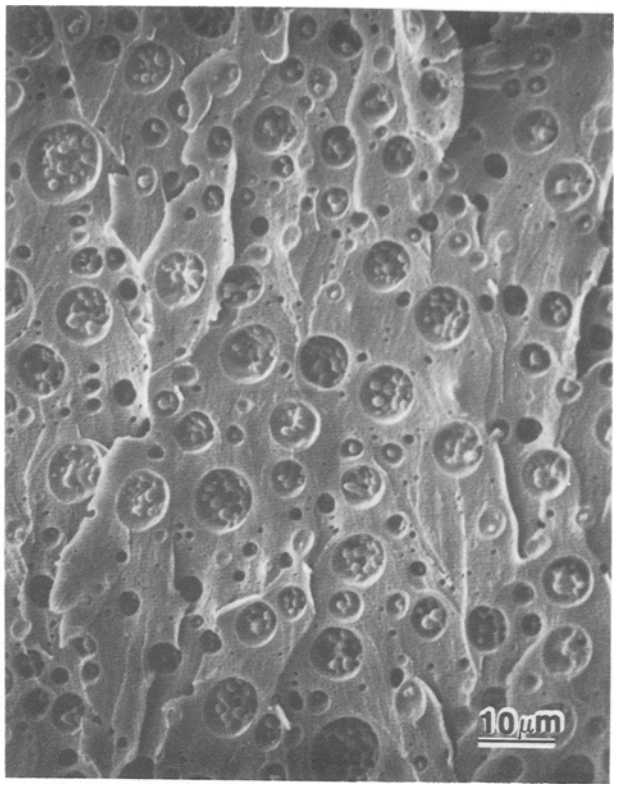

Figure 15 SEM from the stress-whitened area of fractured SEN-3PB specimen of 828-BPA(24)-8(15). Note the glassy occlusions in the fractured rubber particles.

the 828-15 materials. The cavities for the 828-8 epoxies are quite smooth and featureless. Actually, the cavity walls are lined with a layer of rubber. This will be shown to be the case when the backscattered electron analysis is presented. Then, the rubber particles appear to have cavitated and then "ballooned-out" with the growing void in the matrix. The difference in the morphology of the fractured rubber particles between 828-15 and 828-8 is perhaps due to a greater crosslink density of the latter since its acrylonitrile content, hence DGEBA solubility, is greater. Despite these differences in the fracture surface morphology of these two types of rubber, the fracture toughness values of these two systems are comparable (see [1]). These observations suggest that the rubber type is not very important, as long as it is able to form a distinct dispersed phase.

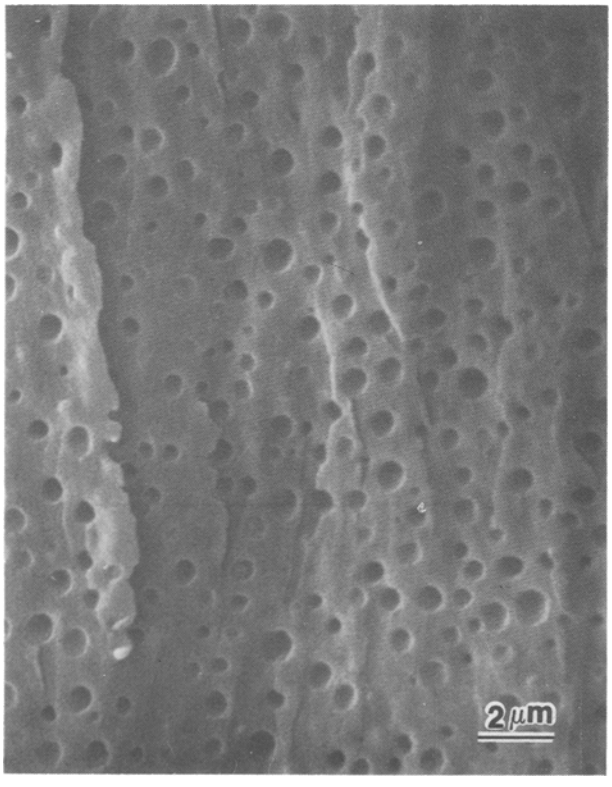

Figure 14 SEM from the stress-whitened area of fractured SEN-3PB specimen of 828-BPA(24)-8(10).

The fracture surface of the BPA modified epoxy is also dependent upon rubber content. At 5 and 10 phr the rubber particles form a distinct single phase. The SEM micrographs from the SEN-3PB fracture surface in the stress whitened region show cavities similar in appearance to those of the 828-8 system except that they are much smaller in size (see Figs 13 and 14). At 15 phr rubber, large multiphase particles approximately 10 μm in diameter are formed. These particles have a "salami"-type structure similar to that found in high impact polystyrene. At this rubber content these particles are within one diameter of each other; furthermore, very small (approximately 0.1 μm) particles populate the interstitial space between the large particles. Figs 15 to 18 are higher magnification SEM micrographs from the stress-whitened and fast fracture regions, respectively, of the SEN-3PB fracture surface of 828-BPA(24)-8(15). These SEM micrographs reveal the now-familar difference in the depths of the cavities in the two regions. Note that the submicron cavities in the interstitial space between the larger cavities do not appear to be smeared out or otherwise show signs of enhanced plastic flow on this scale. The source of enhanced toughness of this system

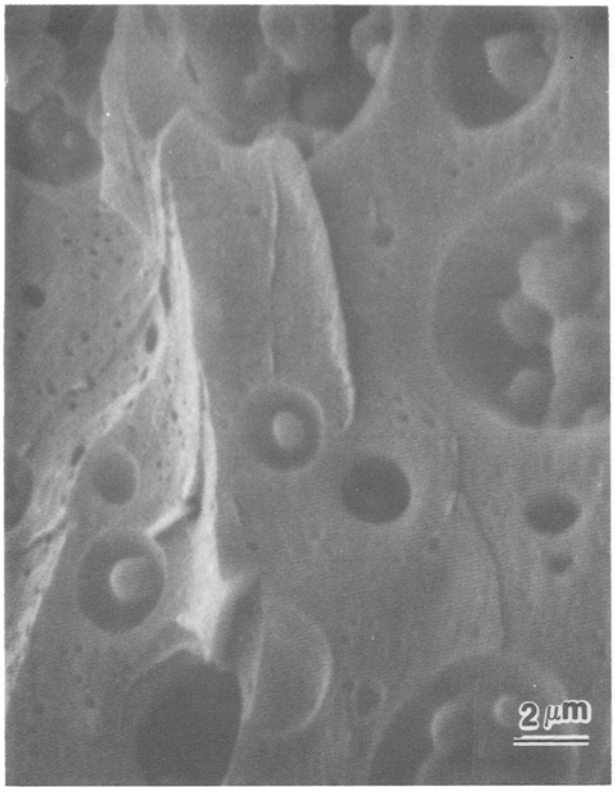

Figure 16 Higher magnification SEM of the fracture surface in Fig. 15. Note the cavities formed by the small particles in the interstitial space between the large particles.

may thus lie in the higher ductility on a much grosser scale.

Observations of the fracture surfaces by SEM can easily lead one to the conclusion that the cavities are all that remains after the rubber particles have somehow been ejected from the fracture surface. To determine whether the cavities are rubber-lined or empty, a backscattered electron imaging technique was employed. This technique measures the extent to which electrons are elastically scattered from the surface. Contrast between the epoxy matrix and the elastomer phase is obtained by OsO_4 staining. OsO_4 preferentially adds only to the unsaturated elastomer. Since osmium has a significantly larger scattering cross-section than organic polymers, it can be readily detected by producing a higher intensity of backscattered electrons. Figs 19 to 21 are SEM micrograph of OsO_4 stained fracture surfaces of 828-BPA(24)-8(15), 828-8(10), and 828-15(10), respectively, using the backscattered electron imaging technique. The osmium stained regions appear light in these micrographs. In Fig. 19, the internal structure of the rubber particles in the BPA-modified epoxy is clearly discernible, yet details of the fracture surface are lost. The cavities found on the fracture surfaces of the other two systems are likewise shown to be lined with rubber.

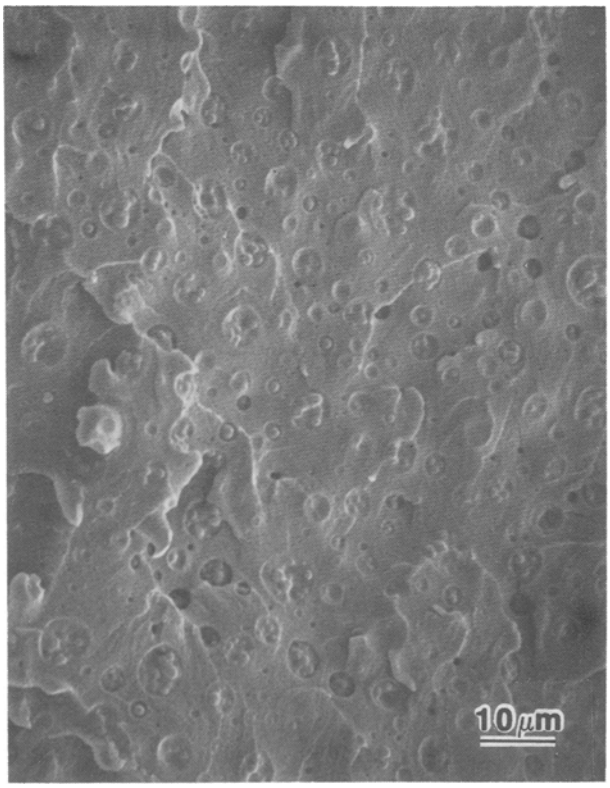

Figure 17 SEM from the fast fracture area of fractured SEN-3PB specimen of 828-BPA(24)-8(15). Compared with Fig. 15, the cavities are shallower and the cavity diameters are smaller.

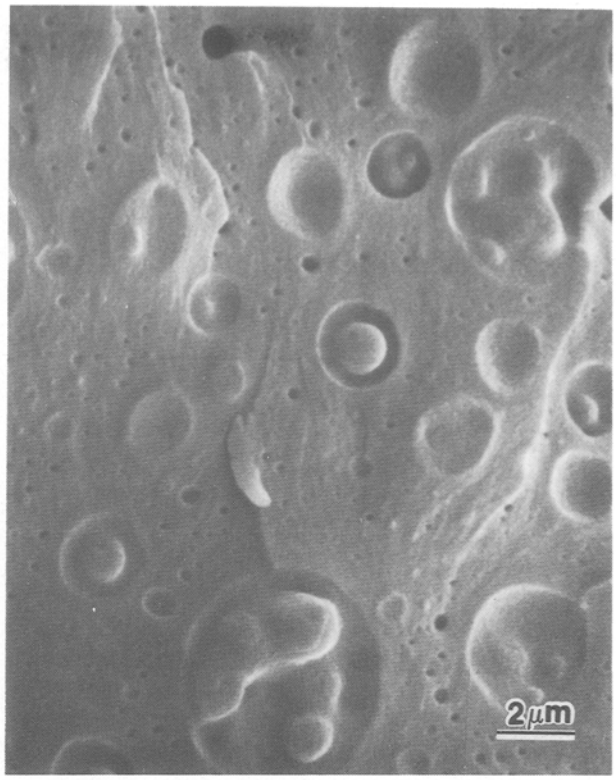

Figure 18 Higher magnification SEM of the fracture surface in Fig. 17.

The use of tensile tests to investigate toughening mechanisms in plane strain fracture is predicated upon the argument that the deformation mechanisms are similar in both cases. This argument should be correct for tensile cracks that mainly propagate in a plane. Direct SEM evidence to support this similarity are presented here.

Figs 22 to 24 contain SEM micrographs of the slow crack growth regions of the tensile fracture surfaces of the 828-15 system containing various amounts of rubber. Although not as large as those in the stress-whitened zone of the SEN-3PB specimen, the diameters of these voids are generally larger than those of

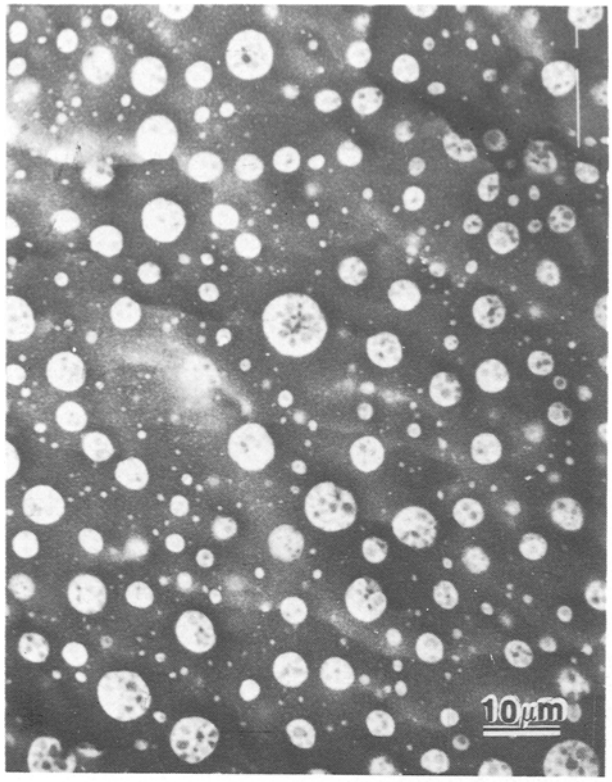

Figure 19 SEM in the back-scattered electron mode from the same type of fracture surface as in Fig. 15. The fracture surface has been stained with OsO_4. The rubber particles appear lighter than the epoxy because the osmium is concentrated on the unsaturated rubber.

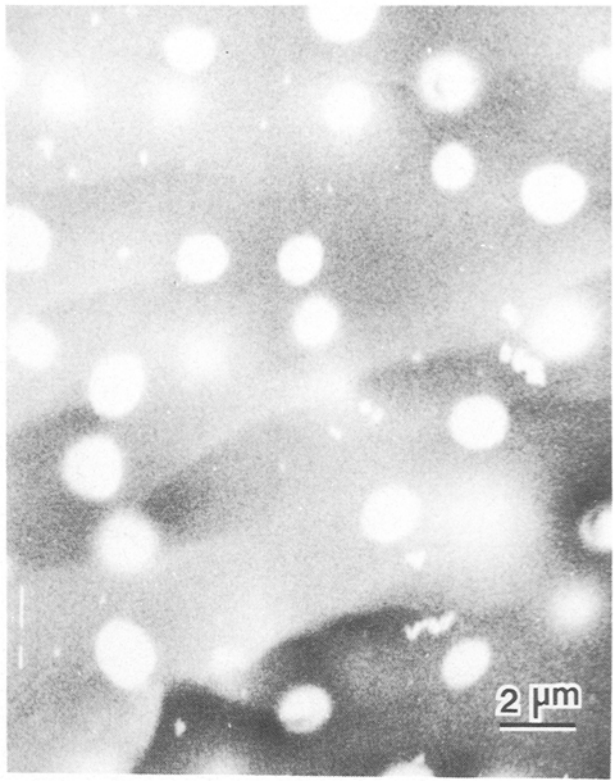

Figure 21 SEM in the back-scattered electron mode from the fracture surface of 828-8(10). The fracture surface has been stained with OsO_4.

Figure 20 SEM in the back-scattering electron mode from the fracture surface of 828-15(10). The subsurface rubber particles are faintly visible because the OsO_4 stain can penetrate beyond the surface.

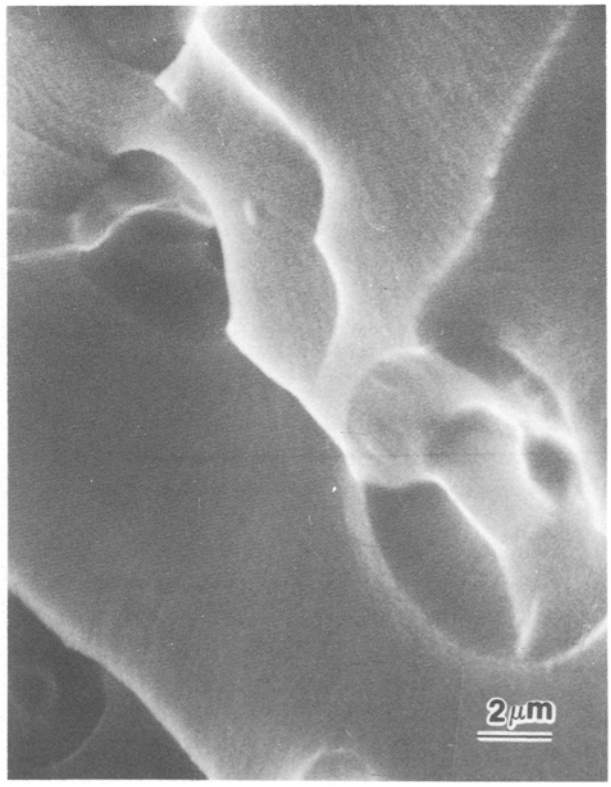

Figure 22 SEM from the slow crack growth area of a fractured tensile specimen of 828-15(10).

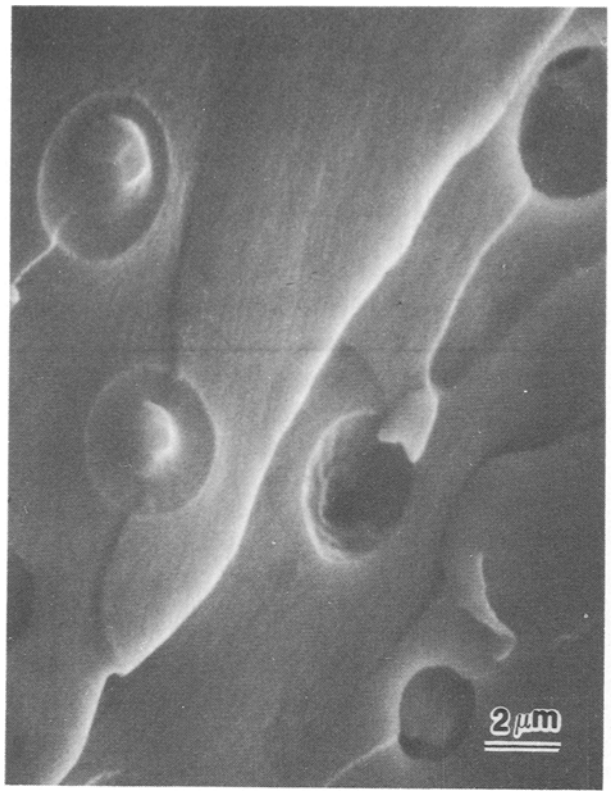

Figure 23 As in Fig. 22, but for 828-15(15).

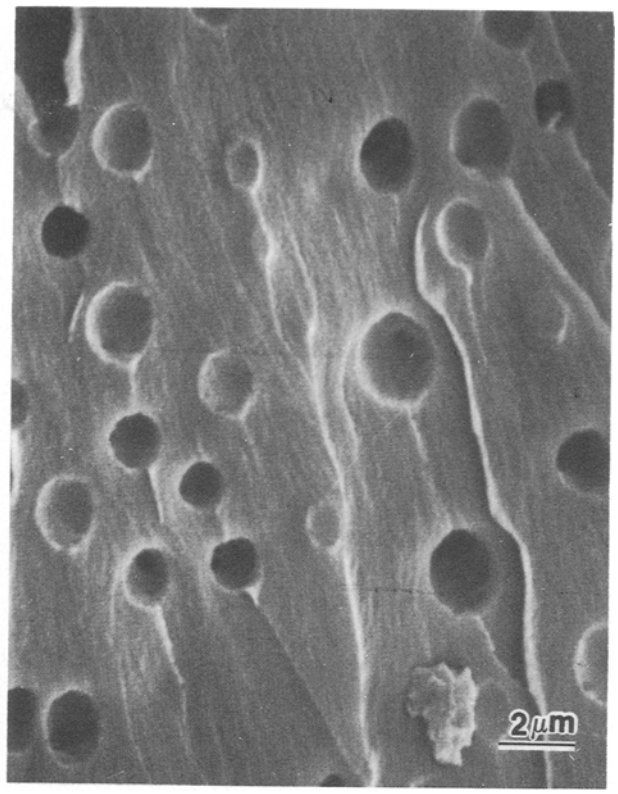

Figure 25 SEM from the slow crack growth area of a fractured tensile specimen of 828-8(10).

the undeformed particles. In the tensile case the particles appear to have failed in a "cup and cone" type of fracture, presumably after a cavity has been initiated in the centre of the particle. However, these cup and cone pairs appear to be in turn surrounded by disc-shaped cavities which originally may have been deeper just prior to total separation, but have recovered some of the deformation afterwards. Note that the epoxy matrix around these voids is very flat, in contrast to the bevelled edges in the SEN-3PB specimens.

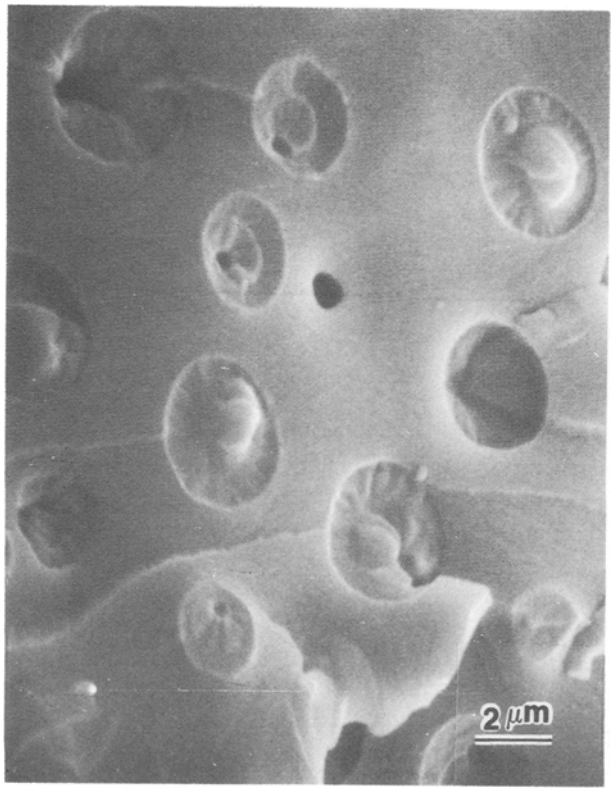

Figure 24 As in Fig. 22, but for 828-15(20). Note that the cavity diameters are smaller than those in Fig. 23. This is because at this level of rubber and strain rate, the deformation is essentially by shear.

Figs 25 to 28 are SEM micrographs from both the slow and fast crack growth regions of tensile specimens of 828-8. The fractured rubber particles in SEN-3PB and tensile specimens are virtually indistinguishable from each other.

In spite of the differences noted, the tensile and SEN-3PB fracture surfaces are quite similar, thus lending credence to the ability of the tensile dilatometry experiment to model fracture toughening mechanisms. The energy dissipation processes observed in these SEMs are: the cavitation and fracture of the rubber particles, and the dilation and plastic deformation of the surrounding matrix at the surface.

The fact that stress-whitening is visible on most of the fracture surfaces indicates that a damage layer in at least the micrometre range in thickness undoubtedly exists. However, the nature of the subsurface damage cannot be unambiguously determined from the SEM of fracture surfaces. For example, remnants of broken craze fibrils are usually extremely difficult to view on the fracture surface. Shear bands do not usually produce sufficiently sharp surface topography. The following discussion is devoted to investigations of subsurface damage by OM and TEM.

3.2. Optical microscopy

OM is particularly useful for observing deformations that induce birefringence. Thus thin sections perpendicular to the fracture surface of SEN-3PB specimens

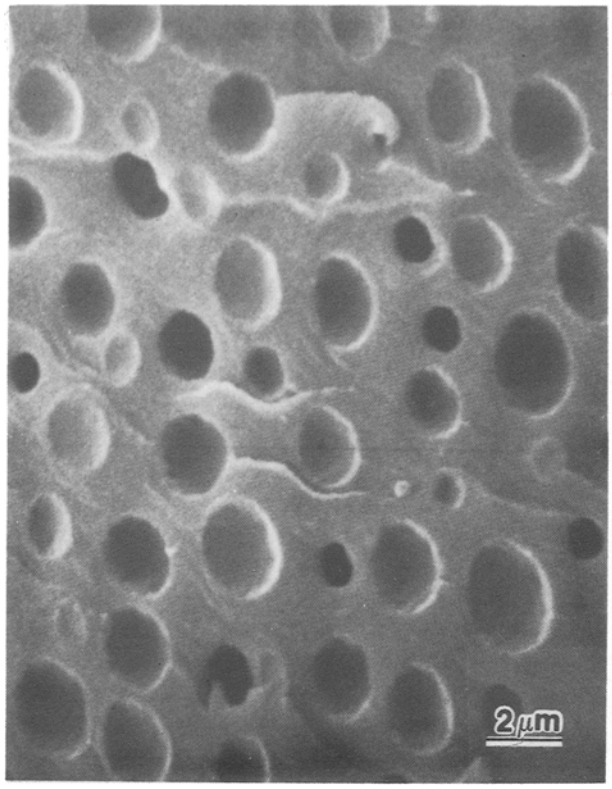

Figure 26 As in Fig. 25, but for 828-8(20).

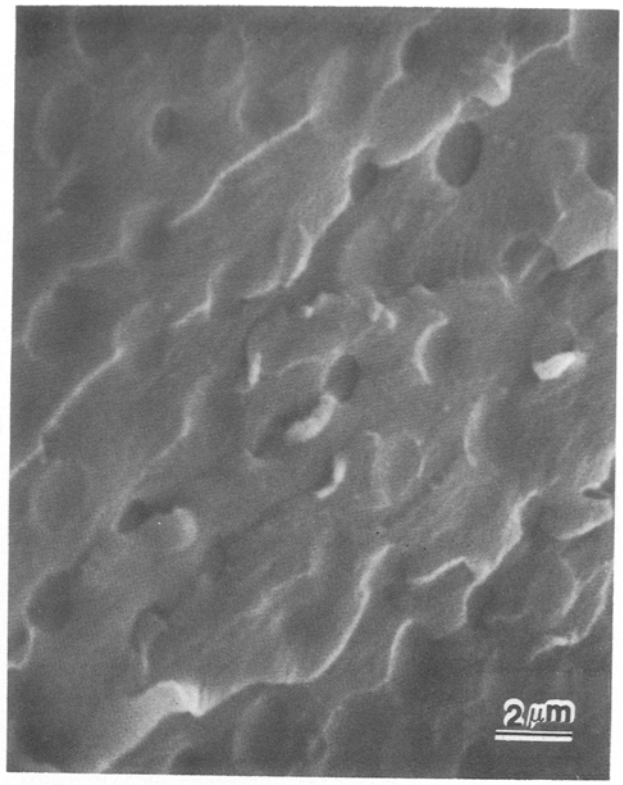

Figure 28 As in Fig. 26, but from the fast fracture area.

are viewed in an optical microscope to elucidate the nature of the subsurface damage zone.

Figs 29 and 30 are optical micrographs from SEN-3PB specimens of 828-8(20) and 828-BPA(24)-8(15), respectively. These micrographs show a strongly birefringent damage zone that is from 100 to 150 μm in thickness. Fig. 30 shows a fracture surface that contains many steps, indicating that the crack has travelled along different planes. Figs 31 and 32 are higher magnification micrographs taken from the same two specimens, respectively. The fracture surface in Fig. 32 is at the upper right hand corner. In these micrographs, thick bands of highly birefringent material are seen to meander from particle to particle. These bands are as a whole not parallel to the plane of the fracture. Further away from the fracture surface, where there are fewer bands, it is easier to see that these birefringent bands are distinctly inclined with respect to the fracture surface. The inclination of these bands is characteristic of shear bands. Near the fracture surface, the rubber particles appear to be significantly larger than those outside the plastic zone. The limited resolution of OM makes it impossible to ascertain the exact size of these enlarged particles, nor is it possible to determine if cavitation has occurred. But cavitation

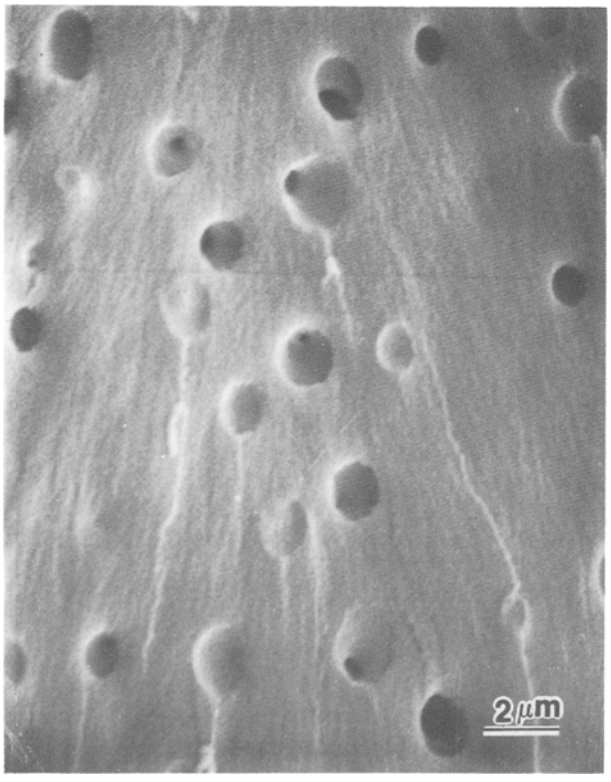

Figure 27 As in Fig. 25, but from the fast fracture area.

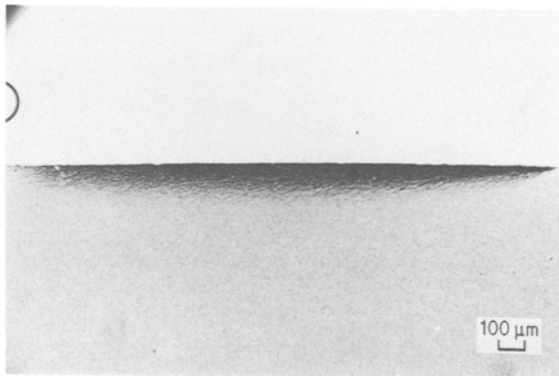

Figure 29 Bright-field OM of thin section perpendicular to the fracture surface showing subsurface damage in SEN-3PB specimen of 828-8(20). The crack ran from right to left. The dark region is the plastic zone caused by voids and shear bands.

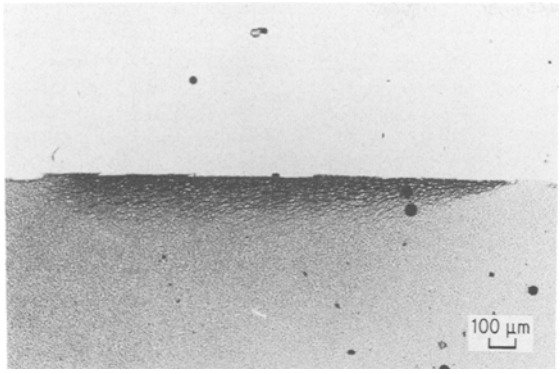

Figure 30 As in Fig. 29, but for 828-BPA(24)-8(15). Note the larger plastic zone corresponding to higher toughness.

or debonding of the particles must have occurred, judging by the intense stress whitening.

Some of the particles in Fig. 32 are quite large, and they contain subinclusions. This feature has already been observed earlier using SEM. The particles near the fracture surface are slightly elongated; they scatter light whenever the birefringent bands pass through them. The scattering is due to internal voiding. Again the limited resolution of OM does not allow the precise determination of these features. Here, too, the intense stress whitening indicates that voiding or debonding must have occurred. Near the fracture surface (upper right hand corner), the bands coalesce so that they form patches of birefringence. In the black and white photographs shown, they have a mottled appearance..

Figs 33 to 36 are transmission optical micrographs of the subsurface damage zone from 828-15(10) SEN test specimens and tensile specimens. The lower rubber content and large rubber particles bring out certain features obscured in the higher rubber content systems. Fig. 33 is a bright field micrograph of the subsurface damage in a fractured tensile specimen. Here, internally voided rubber particles appear black due to the diffraction of visible light by the voids. This same section, when viewed between crossed polarizers, is shown in Fig. 34. The highly birefringent bands radiating from the voided rubber particles are distinctly shear bands. These micrographs provide further evidence for the proposed toughening mechanism, i.e. internal voiding and enhanced shear band formation. Figs 35 and 36 are transmission optical micrographs of the subsurface damage of a fractured SEN specimen. Again, the same two types of mechanisms are observed: internal voiding and shear band formation. These results support the assumption that the deformations measured by tensile dilatometry [1] are similar to the deformations occurring at the crack tip.

An important observation pertaining to the sequence of deformation events can be made up studying Figs 31, 32, 35 and 36. In the region far away from the fracture surface, where the stress is lower, only voiding is observed. By comparison, in the region closer to the fracture surface, where the stress is relatively higher, both voiding and shear banding are observed. Thus, it can be unambiguously concluded that voiding precedes shear banding. In fact, it can be deduced that the voids enhance shear band formation. This can be understood in terms of the stress concentration caused by the voids, which shortens the relaxation time in a highly localized manner [1, 6].

To sum up the OM observations, the formation of thick plastic zones appear to be associated with the presence of a high volume fraction of rubber particles. Close proximity of the rubber particles to each other appears to enhance the formation of shear bands between the particles. Particle–particle interaction is thus indicated. These bands have none of the characteristics conventionally associated with crazes in thermoplastics. The bands always pass through particles that diffract light, but not all particles that diffract light have bands emanating from them. The light diffracting property of the particles is most likely caused by internal cavitation. Thus, the deformation process is one of cavitation of the particles followed by shear bands that form between the particles.

The cavitation of the rubber particles observed by

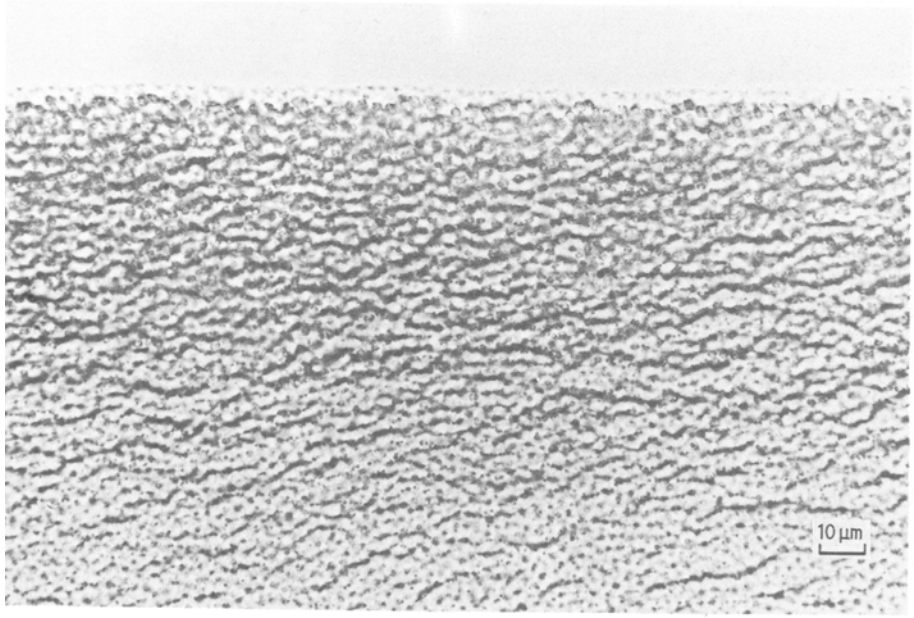

Figure 31 As in Fig. 29, but at a higher magnification. The rubber particles near the fracture surface are cavitated more than those further away from the fracture surface. The density of the shear bands is also higher near the fracture surface.

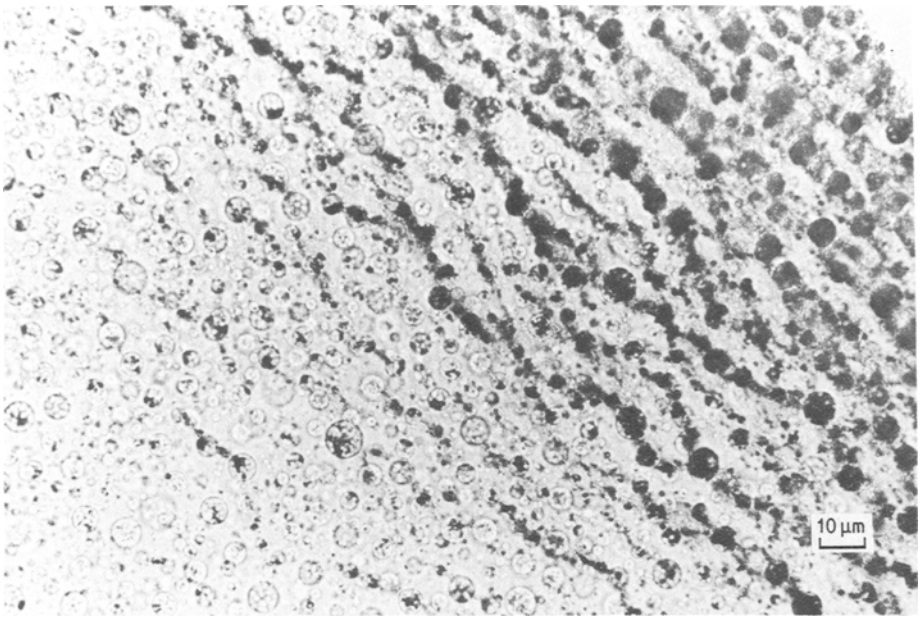

Figure 32 As in Fig. 30, but at a higher magnification and viewed between crossed polarizers. The fracture surface is at the upper right hand corner. The cavitated particles appear dark because of light diffraction. Near the fracture surface the cavitated particles are also somewhat elongated. Shear bands, which are birefringent, span the particles. The rubber particles furthest away from the fracture surface (lower left hand corner) are not cavitated. In the intermediate zone the cavitated particles are not always associated with shear bands.

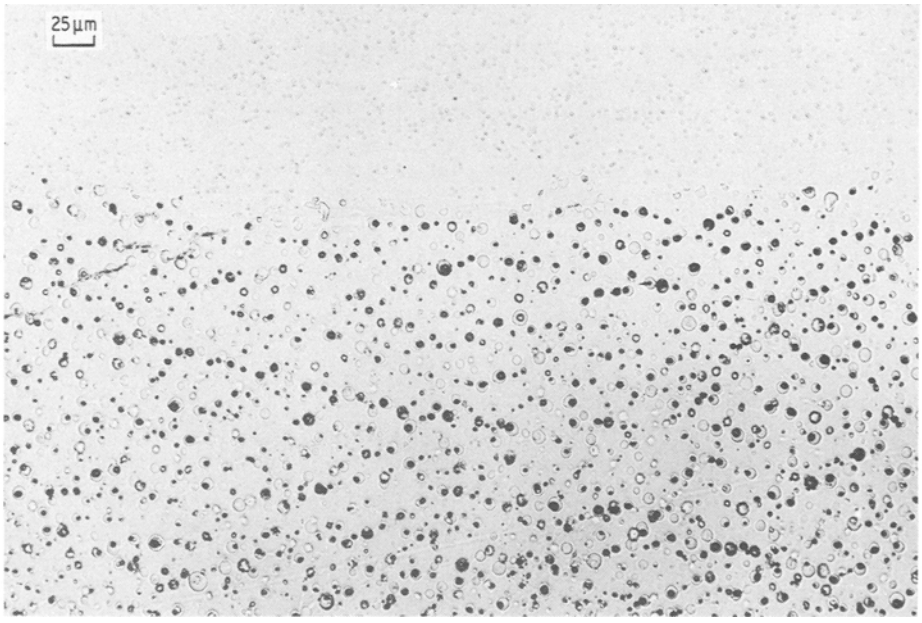

Figure 33 Bright-field OM of thin section perpendicular to the fracture surface of a tensile specimen of 828-15(10). The cavitated rubber particles are dark because of light diffraction.

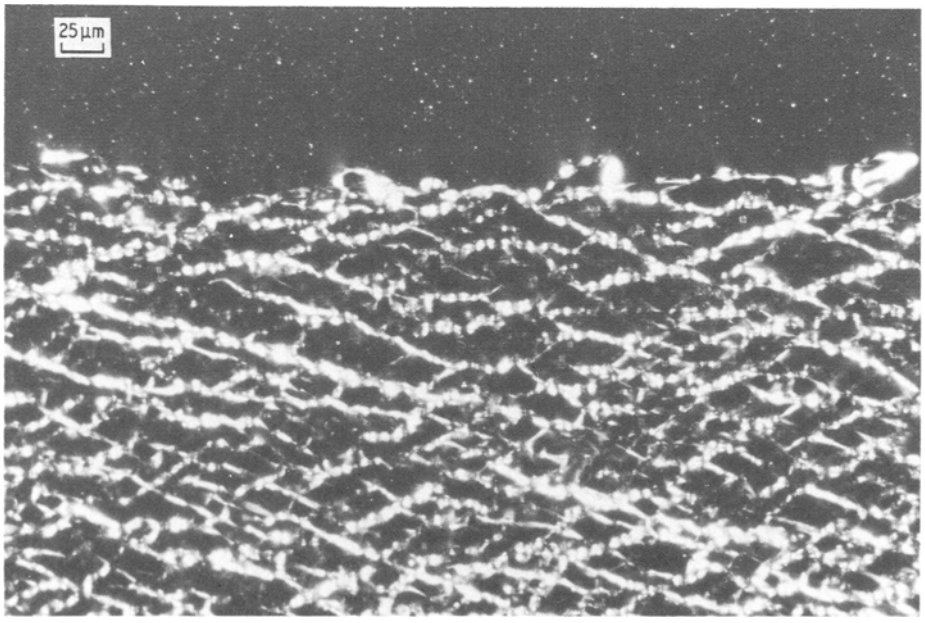

Figure 34 The same thin section in Fig. 33 viewed between crossed polarizers. The shear bands are highly birefringent and appear as bright bands. Not all the cavitated particles in Fig. 33 are associated with shear bands.

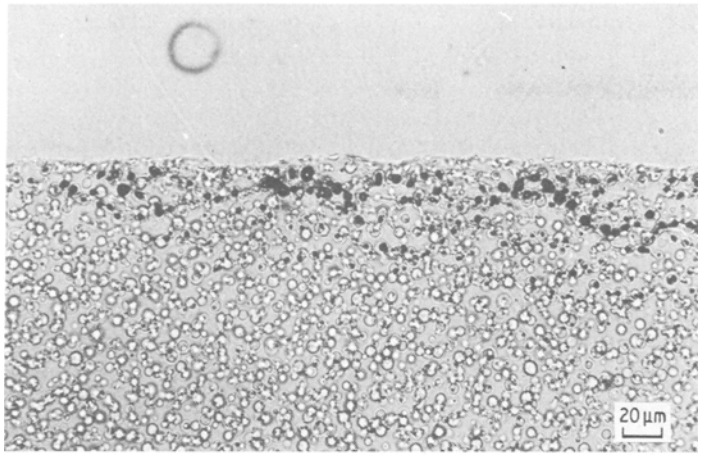

Figure 35 Bright field OM of thin section perpendicular to the fracture surface of a SEN-3PB specimen of 828-15(10). The cavitated rubber particles are confined to a zone near the fracture surface.

OM can be corroborated by TEM of sections microtomed perpendicular to the fracture surface. A typical TEM micrograph is shown in Fig. 37. With few exceptions, the rubber particles are torn easily from the matrix, apparently during the microtoming, if they are very near the fracture surface. But the OsO_4 stained rubber particles far away from the surface are cut without any tearing. This indicates that the particles near the surface have much lower mechanical integrity prior to the microtoming. It can be surmized that they have undergone cavitation or debonding. The matrix exhibits no crazing or voiding of any kind. It is possible that the technique used in sample preparation is not sufficiently refined to allow extremely small voids or crazes to be observed. What is more likely, though, is that these types of deformations, if they exist, are not at all prevalent.

The deformation process during crack propagation can be hypothesized from the above observations. It appears that the sharp starter crack is first blunted by a plastic zone which grows as the stress is increased. Due to the constraint in the centre of this zone, a triaxial tensile stress is generated, resulting eventually in cohesive failure of the rubber particles along a plane perpendicular to the major principal tensile stress. Thus the initial plastic zone that blunts the start crack consists of a voided material. But as soon as the shear bands form they become the dominant mode of deformation, causing the plastic zone to grow further. According to this hypothesis, then, the principal energy absorbing mechanism appears to be shear banding, which is made possible by the voids formed by the cavitated rubber particles.

4. Conclusions

A myriad of deformation mechanisms have been observed in these studies: the rubber particles cavitate and fracture; the resultant voids in the matrix grow and coalesce; finally, the matrix also forms shear bands. These observations are in agreement with the volume strain measurements of Part 1 [1] where cavitation and shear banding were deduced as the two major deformation mechanisms.

The existence of crazes in the conventional sense regarding thermoplastics cannot be verified in these experiments. They have not been found unambiguously in the dilatometric studies, nor by using TEM techniques that in the past have been successful in locating crazes. Certainly, no evidence for massive crazing exists. These results contradict the conclusion of Bucknall and Yoshii [7], Sultan and McGarry [8], and Riew and co-workers [5, 9, 10]. It should be emphasized that the possible existence of isolated crazes in crosslinked epoxies is not being discounted by the foregoing discussion. Based on available evidence, however, crazing is not an important energy dissipation mechanism in the toughening of these epoxies.

The rubber particles undoubtedly also stretch and tear; but, at least in the systems studied here, not to the extent observed by Kunz and Beaumont [11–13]. By themselves these rubber particles probably absorb relatively little energy – even Kunz and Beamont's

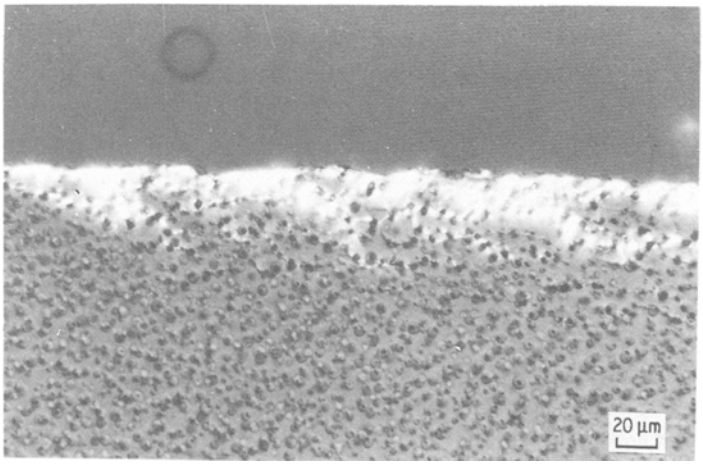

Figure 36 The same thin section in Fig. 35 viewed between crossed polarizers. The birefringent shear bands are confined to an even narrower zone near the fracture surface than the cavitated particles.

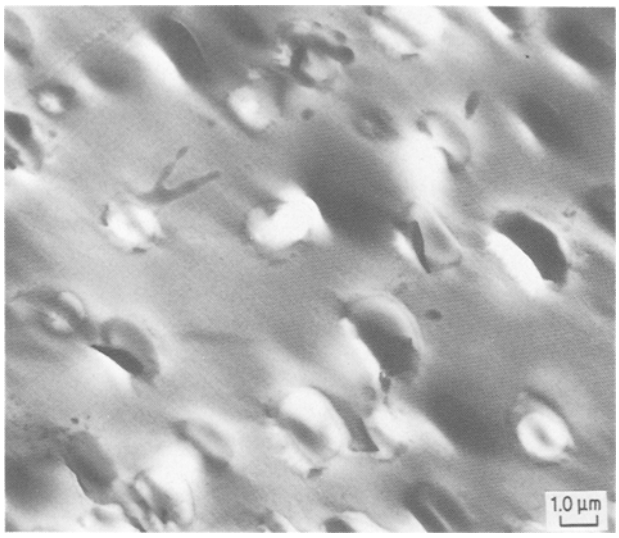

Figure 37 TEM of OsO_4 stained thin section of a SEN-3PB specimen. The fracture surface is near the top of the micrograph. The rubber particles, which appear dark due to the staining, are cavitated.

model calculations show a contribution of only several hundred J m^{-2} at high rubber contents. Nevertheless, the particles appear to play an important role.

The difficult process of nucleating voids in a solid has apparently been facilitated by the presence of the rubber particles. Once formed the voids grow and dissipate bulk strain energy. They also concentrate stresses, and depending on the stress configuration and volume fraction cause either ductile fracture of the ligaments between adjacent voids aligned perpendicular to the major principal tensile stress, or cause shear localization (shear bending) to occur. They enable the formation of large plastic zones, which probably absorb most of the energy. These conclusions are in accordance with those of Bascom and co-workers [14–17], and Kinloch *et al.* [18].

Ultimately, the toughness of the material lies in the ease with which the matrix can deform in shear, though not necessarily to form narrow and sharp shear bands. It seems reasonable to state that one helpful property would be a high Poisson's ratio, for then a higher proportion of the strain energy goes into shear. A high Poisson's ratio in a real solid does not mean that it is incompressible, merely that the bulk modulus is high relative to the shear modulus. It is not clear how the molecular structure of a glass relates to its Poisson's ratio. The effect of crosslink density, though, is perhaps easier to predict. Increasing the crosslink density should increase the bulk modulus much less rapidly than the shear modulus; thus, a lower crosslink density appears to be preferred from this standpoint. The effect of crosslink density will be addressed in a subsequent paper (Part 3).

Acknowledgements

The authors wish to acknowledge the generosity of Dr K. Riew of B. F. Goodrich, Co., for providing the liquid rubbers and a plaque mould free of charge. Mr C. Lizak kindly provided first hand information on the preparation of the epoxy plaques.

The authors are indebted to numerous scientists at the General Electric Research and Development Center for advice, help and discussions on techniques and results.

Dr C. B. Bucknall of the Cranfield Institute of Technology generously gave of his invaluable experience and advice.

Finally, the authors wish to thank Dr N. Johnston of NASA-Langley, the Contract Monitor of this work, for his encouragement. This work was partially funded by NASA Contract NAS1-16132.

References

1. A. F. YEE and R. A. PEARSON, *J. Mater. Sci.* **21**, (1986) 000.
2. S. Y. HOBBS and V. H. WATKINS, *J. Polym. Sci.* **20** (1982) 651.
3. A. S. TETELMAN and A. J. MCEVILY Jr, in "Fracture of Structural Materials" (Wiley, New York, 1967) p. 50.
4. A. S. HOLIK, R. P. KAMBOUR, S. Y. HOBBS and D. G. FINK, *Microstruct. Sci.* **7** (1979) 357.
5. C. K. RIEW and R. W. SMITH, *J. Polym. Sci. A1* **1** (1971) 2739.
6. A. F. YEE, R. J. BANKERT, K. L. NGAI and R. W. RENDELL, *J. Polym. Sci., Polym. Phys. Ed.* in press.
7. C. B. BUCKNALL and T. YOSHII, *Brit. Polym. J.* **10** (1978) 53.
8. J. N. SULTAN and F. J. MCGARRY, *J. Polym. Sci.* **13** (1973) 29.
9. C. K. RIEW, E. H. ROWE and A. R. SIEBERT, *ACS Adv. Chem. Ser.* **154** (1976) 326.
10. E. H. ROWE, in Proceedings of the International Conference on Toughening Plastics, London, 1978, (Plastics and Rubber Institute) p. 23.
11. S. KUNZ, PhD thesis, University of Cambridge (1978).
12. S. C. KUNZ-DOUGLASS, P. W. R. BEAUMONT and M. F. ASHBY, *J. Mater. Sci.* **15** (1980) 1109.
13. S. C. KUNZ and P. W. R. BEAUMONT, *ibid.* **16** (1981) 3141.
14. W. D. BASCOM, R. L. COTTINGTON, R. L. JONES and P. PEYSER, *J. Appl. Polym. Sci.* **19** (1975) 2545.
15. *Idem, J. Adhesion* **7** (1976) 333.
16. W. D. BASCOM, R. L. COTTINGTON and C. O. THOMAS, *J. Appl. Sci.: Appl. Polym. Symp.* **32** (1977) 165.
17. W. D. BASCOM, R. Y. TING, R. J. MOULTON, C. K. RIEW and A. R. SIEBERT, *J. Mater. Sci.* **16** (1981) 2657.
18. A. J. KINLOCH, S. J. SHAW, D. A. TOD and D. L. HUNSTON, *Polymer* **21** (1983) 1341.

Received 29 July
and accepted 18 September 1985